Project 071 Predictive Simulation of nvPM Emissions in Aircraft Combustors

Georgia Institute of Technology

Project Lead Investigator

Suresh Menon, Professor
School of Aerospace Engineering
Georgia Institute of Technology
270 Ferst Drive, Atlanta, GA 30332-0150
(404) 894-9126
suresh.menon@aerospace.gatech.edu

University Participants

Georgia Institute of Technology

- PI: Dr. Suresh Menon
- FAA Award Number: 13-C-AJFE-GIT-067
- Period of Performance: October 1, 2020 to September 30, 2022
- Overall Task(s):
    1. **Kinetics** Modeling: Improvements in soot kinetic model to predict development of polycyclic aromatic hydrocarbon (PAH) pathways in representative sooting fuels.
    2. **Nucleation Modeling**- Simulation of PAH rings at a range of relevant flame temperatures to identify key species contributing to soot nucleation process.
    3. **Surface Growth and Aggregation Modeling** - Reaction-transport-limited growth of soot particles models for cluster–cluster aggregation
    4. **Large-Eddy Simulations (LES)**- coupling the multi-scale models developed in Tasks 1-3 in a method of moment LES method for soot–turbulence–chemistry interactions with application to canonical flames

Project Funding Level

Current FAA funding is for a 2-year effort (July 2020 to September 2022), with a request of $500,000 per year from ASCENT (per year). Additional funding for year 3 is requested. Cost share is provided by:

- Georgia Tech provides cost-sharing for their share of $150,000 per year. The Georgia Tech point of contact is Kevin Ellis (kevin.ellis@aerospace.gatech.edu).
- Raytheon Technologies Research Center (RTRC) provides cost-sharing of $250,000 per year. Dr. Colket is a consultant in this project with many years of experience in soot modeling. The RTRC contact is John LaSpada (LaSpadJW@RTRC.utc.com).
- UM provides cost-sharing in the amount of $100,000 per year. The UM point of contact is Alexandra Thebaud (thealexi@umich.edu).

Investigation Team

- Dr. Suresh Menon, Georgia Tech: PI, Task 4
- Dr. Miad Yazdani, Raytheon Technologies Research Center (RTRC): Co-PI, Task 3
- Dr. Steve Zeppieri, RTRC: Co-PI, Task 1
- Prof. Angela Violi, UM: Co-PI, Task 2
- Dr. Meredith (Med) Colket, Consultant, RTRC: Co-Investigator, Task 1

Project Overview

This project is being used to establish a new multiscale approach to predict soot formation in aircraft combustors. A hierarchy of first-principles simulation methods are being used to account for the multiscale physics of the formation and transport of non-volatile particulate matter (nvPM, also called soot in the literature). The final objective is to use this multiscale approach to model these physics as models in large-eddy simulations (LES) of realistic gas turbine combustors. We target and isolate the layers of empiricisms that currently exist, in for example, particle inception models, the role of precursor species in nucleation, the particle shape assumptions and their impact on surface growth, the sensitivity of predictions to particle size distribution and the ad hoc coagulation/coalescence mechanisms. The team already has all the modeling tools, but a systematic coupling of these tools in a multiscale, multi-physics strategy has yet to be accomplished by any research group. Hence, this study will establish a new predictive capability by integrating these capabilities.

The multiscale and multi-physics layers of collaborations among the cost-sharing groups are summarized in Figure 1 and briefly described herein. The kinetics group at RTRC is conducting a study to understand the role of gas-phase kinetics in predicting important species potentially labeled as soot precursors. The information on reduced kinetics from RTRC is being used by Georgia Tech and UM to evaluate LES performance and the process of nucleation. In the UM study, the propensity of gas-phase species to form dimers (considered the building blocks of soot inception) under flame conditions is being studied. Identification of soot precursors and the rates of formation of soot nuclei will be the output from these studies. This nucleation rate will be provided to Georgia Tech to update the source terms associated with nucleation processes in six-moment approach of method of moment with interpolative coefficients (MOMIC), and the information on the structures of these soot nuclei will be provided to RTRC for modeling of surface growth and aggregation processes. Outputs from the aggregation studies in RTRC in the form of global surface growth and aggregation models will then be fed back to Georgia Tech to update the source term surface growth and aggregation models in the 6-MOMIC approach. Canonical studies are underway at Georgia Tech to provide information regarding the variations in local conditions, such as pressure, temperature, and local equivalence ratios due to turbulence–chemistry interactions; this information should be useful in each stage of the abovementioned studies. LES studies at Georgia Tech will also involve modeling the effects of chemistry–soot–turbulence interactions by using advanced subgrid models including the linear eddy mixing (LEM) model. As a project deliverable (at the end of this research effort), the final assessment of both the existing soot model and the improved soot model will be conducted in canonical flame configurations.

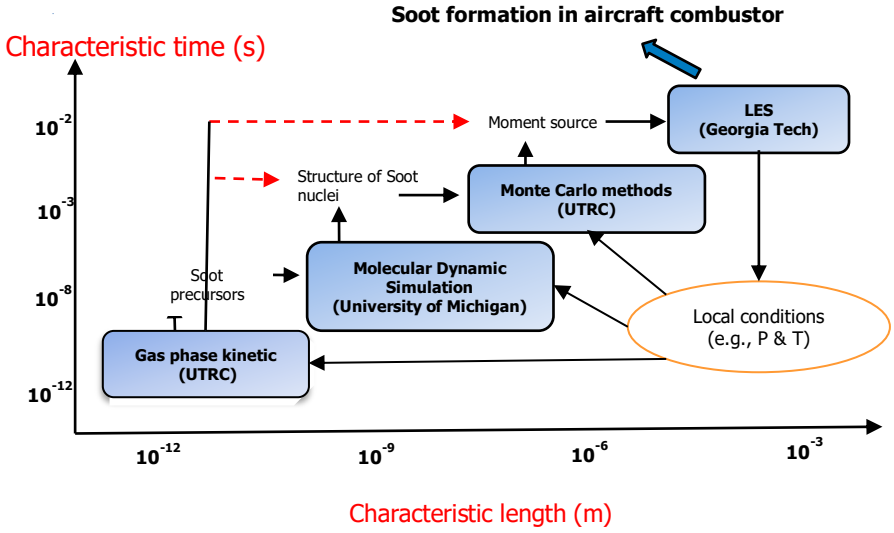

Figure 1. Multiscale collaborative efforts to improve nvPM (soot) predictions.

In the previous report, an overview of all modeling tools and the collaborative efforts to assess inputs and outputs from the analysis at each stage were highlighted, and basic validation and verification were performed to establish capabilities. In the current annual report (for fiscal year 2021), the progress at each stage is briefly described, with particular attention paid to

the main objective of building on the existing approaches for soot modeling and assessing the improvements that could be achieved in each aspect. Key work accomplished by each group is highlighted as separate tasks.

Task 1 - Kinetics Modeling

Raytheon Technologies Research Center

Objective(s)

The objectives of this task are to develop validated detailed and reduced chemical kinetic models of parent fuel decomposition and oxidation reactions, with a special focus on fuel rich chemistry, to enable the accurate evolution of PAH/soot precursor formation and incipient soot particle formation, and the evaluation and improvement of reduced-order soot formation models. Year 1 fuel activities are focused on ethene, and year 2 efforts will focus on Jet-A fuel.

Research Approach

Reduced-Order Soot Model Development

Previous research using canonical datasets (e.g., flow reactor, shock tube, and well-stirred reactor) of ethene oxidation and pyrolysis systems has indicated that, among the published detailed ethene kinetic mechanisms, that of Frenklach (2002) showed the best agreement with the experimental data. Accordingly, that mechanism (101 species and 544 reactions) was chosen for further evaluation against the experimental fuel rich well-stirred reactor studies performed at the Air Force Research Laboratory (AFRL). The skeletal ethene mechanism of Lu and Law (2005) (33 species and 206 reactions) was selected as a reference reduced-order model against which to compare the detailed model. Both mechanisms were coupled to separate particulate formation analysis methods for comparison against experimental soot measurements. The detailed kinetic model used the method of moments soot algorithms, and the reduced chemistry model used the Lindstedt reduced-order soot formation model. The goals of this comparison were to access the viability and limitations of a reduced-order model against detailed PM model results, and to ascertain whether “parameter tweaking” of the reduced model allowed for improved agreement in subsequent computational fluid dynamics (CFD) analysis.

The experimental well-stirred reactor was modeled with the Chemkin perfectly stirred reactor (PSR) code. The test conditions associated with the experiments were 1 atm pressure, reactor residence times of approximately 8.5 milliseconds, and a range of fuel–air equivalence ratios from 1.9 to 2.5. Comparisons of peak reactor temperature and acetylene (C_2H_2) and oxygen (O_2) mole fractions between the detailed and reduced models were 10 K, 30%, and 20%, respectively. These are key parameters used in the soot formation models, as shown in Figure 2.

As shown, acetylene is the key species responsible for soot particle inception and surface growth reactions, and molecular oxygen is the key species for soot oxidation. To close the Lindstedt model (Leung et al., 1991), certain parameters must be defined. The list of these parameters and the values of the parameters recommended by Lindstedt are shown in Figure 3. Because experimental well-stirred reactor data were simulated, the parameter values in the rightmost column for a turbulent system were used.

Lindstedt Soot Model

	Process:	Mass Fraction Rate:	Particle Density Rate:
Inception:	$C_2H_2 \rightarrow 2C_s + H_2$	$R_1 = 2k_1(T)\,[C_2H_2]\,M_s$	$R_4 = \frac{2}{C_{min}} N_A k_1(T)\,[C_2H_2]$
Surface Growth & Oxidation:	$C_2H_2 + nC_s \rightarrow (n+2)C_s + H_2$	$R_2 = 2k_2(T)\,f(S)\,[C_2H_2]\,M_s$	
	$C_s + \frac{1}{2}O_2 \rightarrow CO$	$R_3 = k_3(T)\,S\,[O_2]\,M_s$	
Coagulation:	$nC(s) \rightarrow C_n(s)$		$R_5 = 2C_a\sqrt{d_p}\left(\frac{6\kappa T}{\rho_s}\right)^{1/2}(\rho Y_N)^2$

$k_i = A_i T^{b_i} e^{-E_i/RT}$

S = soot surface area, f(S) ~ $S^{1/2}$

$$\left.\begin{aligned} S &= \pi d_p^2 \rho Y_N \\ d_p &= \left(\frac{6}{\pi}\frac{Y_s}{\rho_s Y_N}\right)^{1/3} \end{aligned}\right\} \Rightarrow S = \pi\left(\frac{6}{\pi\rho_s Y_N}\right)^{2/3} Y_s^{2/3}\rho Y_N$$

Figure 2. Description of the various processes in the Lindstedt soot formation model.

	Fitting Parameters Utilized in Model:	Orig Paper	Second paper
		Laminar Nonpremixed	Turbulent, CrossFlow
		C&F,1987	C&F,1989
Ca	Coagulation Constant	9	3
Cs	# Carbons in Incipient Soot Particle	100	9000
k1-nucleation	A1	10000	1350000
	Ea1/R	21100	20634
k2-surface growth	A2	6000	500
	Ea2/R	12100	12079
k3-oxidation	A3	10000	17800
	n3	0.5	0.5
	Ea3/R	19680	19628

Figure 3. List of fitting parameters in the Lindstedt model and associated values.

A comparison between the experimental data (left side of Figure 4) and the simulation (right side of Figure 4) reveals that the models reasonably represent the order of magnitude of peak soot concentration. The method of moments results better capture the experimental trend of the concentration versus equivalence ratio. The Lindstedt models do not have the correct experimental trend of soot concentration versus equivalence ratio, and the trends are too broad. However, by adjusting the rates associated with the inception and surface growth reactions associated with the model, the equivalence ratio sensitivity to the equivalence ratio is improved. Specifically, the rates associated with each process are set to constant values. These improved results are shown in Figure 5.

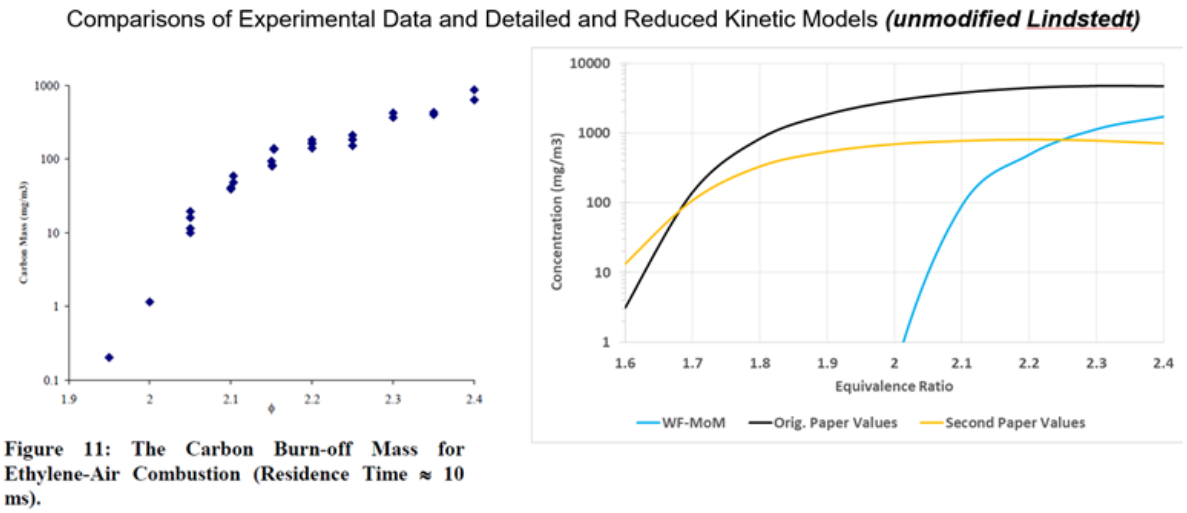

Figure 11: The Carbon Burn-off Mass for Ethylene-Air Combustion (Residence Time ≈ 10 ms).

Figure 4. Comparison of experimental and simulation reactor soot concentration values for the rich ethene AFRL studies.

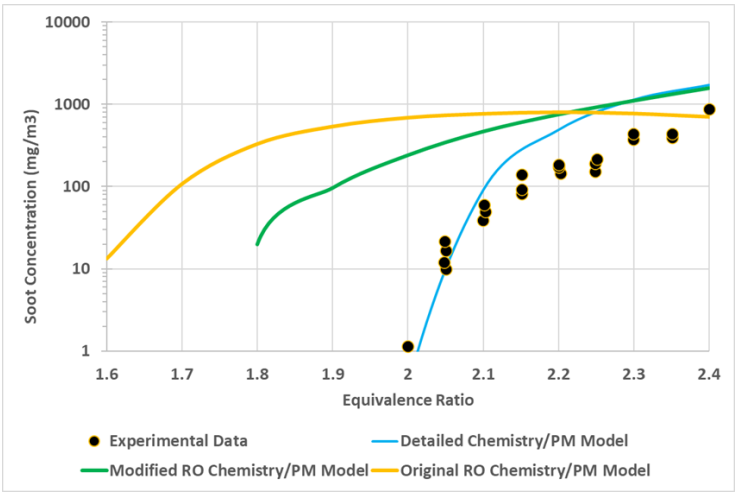

Figure 5. Comparison of experimental and simulation reactor soot concentration values for the rich ethene AFRL studies.

Reduced Kinetic Model Development

An additional task has been to develop a reduced chemical kinetic mechanism for ethene that is sufficiently compact (~25 species) to be used in CFD applications, and contains PAH-related species, such as benzene, naphthalene, and pyrene. These single-ring and multiring aromatic compounds are key soot precursors. Direct calculations within the flow field will enable more detailed physics-based soot inception/growth and transport companion efforts within this project to resolve soot chemistry and physics more accurately.

Mechanism reduction was based on the computer aided mechanism reduction (CARM) technique described by Chen (1988). The Wang-Frenklach detailed mechanism is the input to the CARM tool. A series of Chemkin PSR simulations over a range of parameter space (e.g., pressure, equivalence ratio, and residence time) are computed by using the detailed mechanism. CARM then analyzes these data to determine a prescribed number of species that may be formulated to be in "quasi-steady state" and thus removed from tracking within the reduced kinetic model. An overview of this approach is shown in Figure 6.

CARM* Software Automatically Determines/Generates Necessary Steady State Species Expressions Using Detailed Mechanism Results

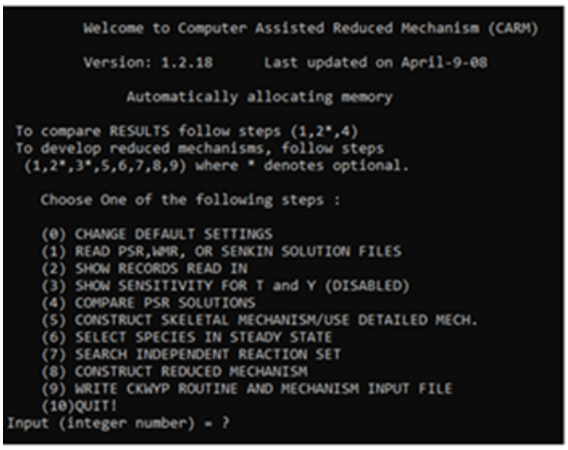

Detailed Model Employed: Wang-Frenklach (98 species/531 reactions)

Target Data Used: PSR Solutions associated with UDRI Reactor Conditions (Φ: 1.9-2.5, 1 atm, τ_{res}: ~8.5 msec)

Goal Outcome: Reduced Mechanism with ~ 25 species, including PAH's (i.e., benzene, naphthalene, pyrene)

Figure 6. Use of CARM and the detailed kinetic mechanism to generate a reduced mechanism.

CARM uses the detailed reactor solutions over the range of target data to rank the errors associated with the quasi-steady-state assumption for each species. After this ranking is established, the number of species sought to be retained in the reduced kinetic model is selected. The code then establishes polynomial based expressions for the non-active species' quasi-steady-state compositional values over the range of target data used. With the above target data, three reduced mechanisms were assembled for comparison against the above AFRL rich ethylene well-stirred-reactor experiments. These mechanisms are shown in Figure 7. These mechanisms were then employed with modified versions of the Chemkin PSR code to compare against the results of both the detailed Wang-Frenklach and reduced Lu mechanisms. Comparisons of major rich products and PAH species are shown in Figures 8 and 9, respectively.

Red. Mech.	Detailed Solutions Used in Build	Phi Range of Detailed Solutions	# Species in Red. Mech.
1	18	1.0-2.5	24
2	10	1.1-2.4	24
3	10	1.9-2.4	23

Figure 7. List of developed reduced mechanisms.

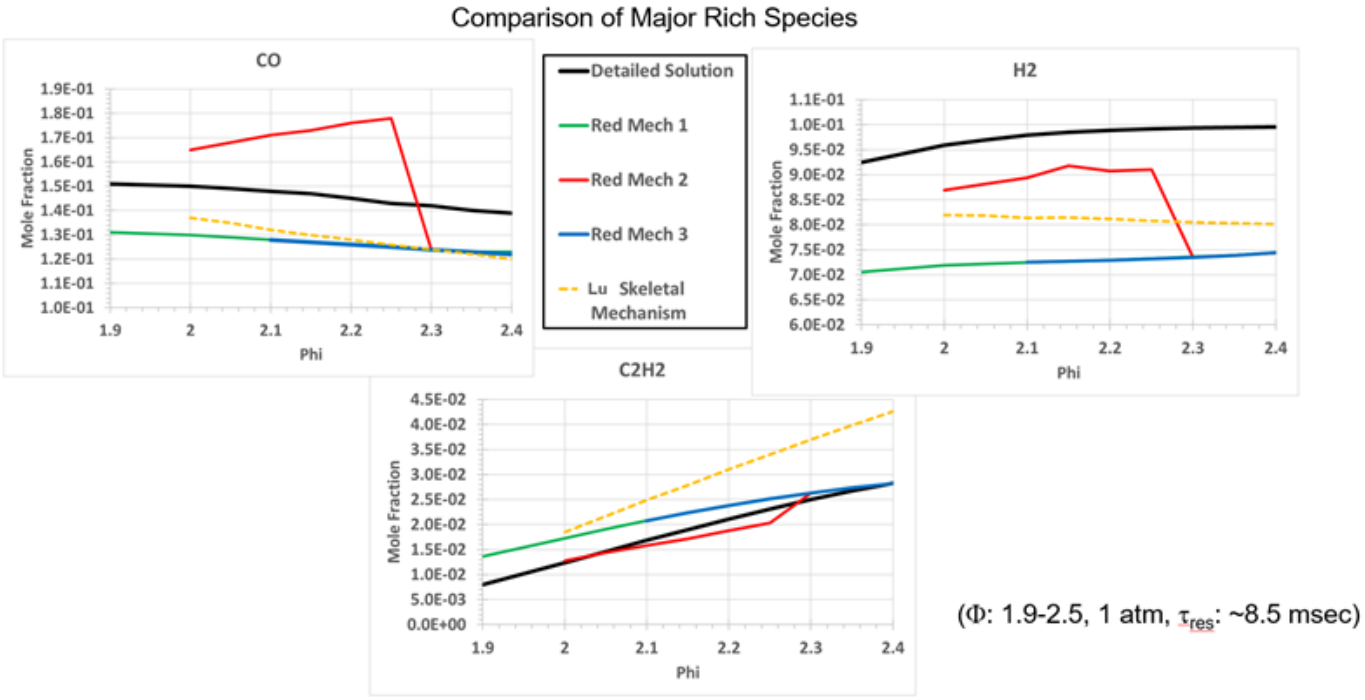

Figure 8. Comparison of major rich species for several Employed mechanisms.

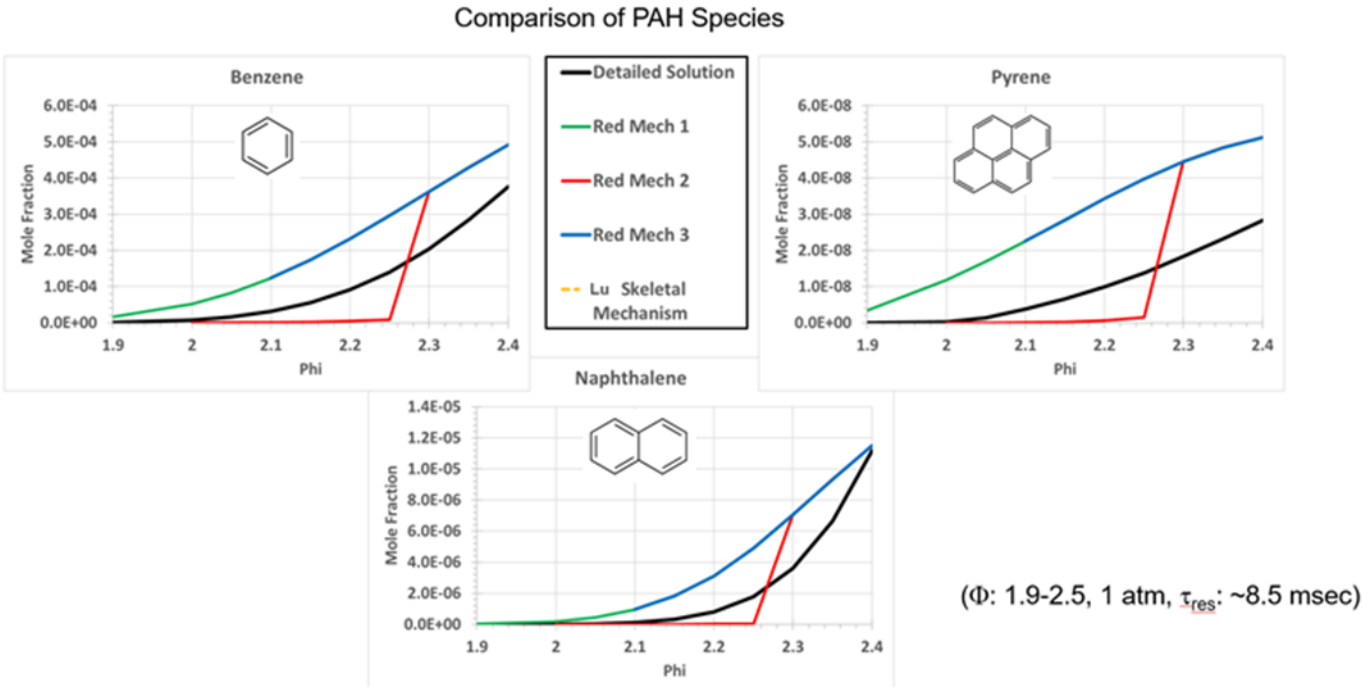

Figure 9. Comparison of PAH species for several Employed mechanisms.

As shown in Figures 8 and 9, of the three developed reduced mechanisms, the first (Red Mech 1) appears to yield the best agreement with respect to the detailed mechanism results. Its results for the rich species are comparable to those of the Lu reduced mechanism. Both give similar agreement for CO, the Lu mechanism yields slightly better H_2 values, and the current reduced model yields better C_2H_2 values. More importantly, the current reduced model better matches the PAH species associated with the detailed kinetic model than the Lu model (Lu & Law, 2005), simply because the current model is the first reduced mechanism to explicitly contain these PAH-related species.

Next Steps

Methods to better anchor the reduced-order Lindstedt soot model to experimental data will continue to be used and implemented. Analysis and construction methods to develop reduced kinetic models yielding better agreement with the detailed kinetic model results, while retaining necessary PAH species in the active species list, will also continue.

Task 2 – Nucleation Modeling

University of Michigan

Objective(s)

The objective of this task is to develop model(s) for nanoparticle inception, a critical step in predicting emissions. This effort bridges the work on gas-phase chemistry (RTRC) with the model for particle growth (RTRC) and provides inputs for the MOMIC model (GT).

Research Approach

Current models for particle inception are unable to reproduce a variety of experimental data, including molecular structure. This work aims at developing a predictive model for particle inception that can provide accurate chemical and physical growth pathways for PAHs. Molecular dynamics (MD) simulations are used to study the collisions of PAHs and the formation of aromatic dimers leading to soot inception.

These atomistic simulations coupled with advanced sampling techniques are used to study the collisions of PAHs. Free energy calculations provide information on the effect of chemical structure and shape on the tendency to form nuclei. In this quarterly effort, after collaboration with RTRC, PAHs that are critical to inception are identified. A pool of aromatic compounds, such as pyrene, benzopyrene, coronene, ovalene, and circumcoronene, are selected. Some preliminary studies for free energy calculations are conducted at temperatures of 500 K and 1000 K. As shown in Figure 3, at lower temperatures, all PAHs appear to form dimers, although dimer formation by higher PAH rings is more favorable. However, at the higher temperature of 1000 K (typical of flame temperature conditions), only higher PAHs tend to form dimers. This finding suggests that the nucleation model from traditional pyrene precursors does not capture the actual soot inception processes. Some of these MD simulation results have been highlighted by Saldinger et al. (2021).

The current focus is to include additional effects of the shape and chemical composition of PAHs on dimer formation and stability. Preliminary analyses have suggested that the addition of aliphatic chains and oxygen radicals facilitates dimer formation, in terms of the free energy of pyrene molecules. Further steps are underway to include the higher hydrocarbons because dimer stability has been observed to increase with heavier monomers. This investigation will involve close feedback regarding kinetics studies at RTRC, so that the kinetic mechanism is modified in parallel. After the key precursors are identified, the collision rates of these dimers will provide insights into the soot nucleation rates, which can be fed into the GT studies. In addition, the structure of soot nuclei can be used by RTRC to further conduct analysis of soot surface growth.

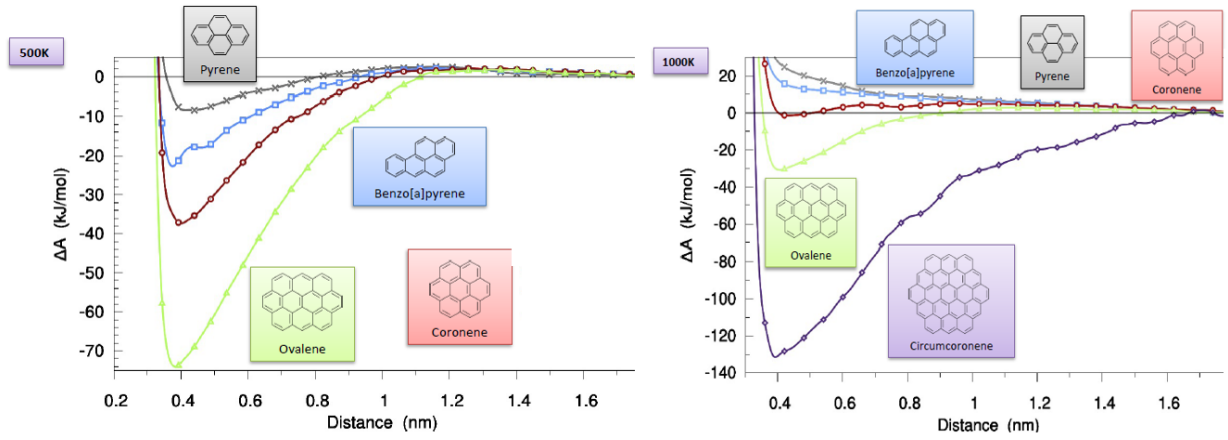

Figure 10. Free energy calculations of PAHs as a function of temperature.

Task 3 - Surface Growth and Aggregation Modeling

Raytheon Technologies Research Center

Objective

The objective is to develop a physics-based framework for the prediction of soot particle growth after the inception process. The growth consists of agglomeration due to collisions between the primary particles and surface growth as a result of direct deposition of the precursors on the aggregate. The final aggregate fractal structure and its temporal evolution as a function of local conditions are of interest. This model will provide the morphology characteristics and the growth rate of the particles as inputs into the MOMIC formulation.

Research Approach

The approach consists of addressing the agglomeration process through diffusion Monte Carlo (DMC) simulation and the growth process through the phase-field method (PFM) simulation. In addition, the transition from a kinetic-limited reaction to a transport-limited reaction as the particle grows will be addressed through matched asymptotic expansion of the coupled concentration/phase-field equation system. The details are provided below.

Agglomeration

The agglomeration of primary particles that leads to the formation of soot is simulated through the DMC approach. Here, the concentration of the primary particles is associated with the concentration of background precursors:

$$\frac{Dc}{Dt} = \frac{\partial c}{\partial t} + \mathbf{u} \cdot \boldsymbol{\nabla} \mathbf{c} = D(p,T)\nabla^2 c + S_a$$

The number density and size distribution of the primary particles are expected to be provided by the MD simulation of the nucleation process. The generated primary particles then go through a random walk according to the background concentration field:

$$P(x',\, t'|x,t) = \frac{1}{\left(4\pi(t'-t)\right)^{d/2}} \exp\left(-\frac{(x'-x)^2}{4D(p,T)(t'-t)}\right)$$

where the diffusivity, $D(p,T)$ is expected to be provided by parametrization of the LES solution. The collision frequency is calculated through $\Delta t = \frac{1}{\beta N}$. After aggregation, the local concentration field is depleted to account for the removal of the

primary particles through aggregation. The depletion is modeled by the addition of a space-dependent sink term in the diffusion equation.

Surface Growth
Surface growth due to direct deposition of background precursors to the cluster is simulated through the PFM. According to the principle of free energy minimization, the phase field, Φ, is effectively a color function for tracking the "deposited" phase. The PFM can ultimately be reduced to the following coupled transport equations (Sun & Beckermann, 2007; Xu & Meakin, 2008):

$$\tau\frac{\partial\phi}{\partial t}=\left\{\varepsilon^2\nabla^2\phi-\frac{\partial f_1}{\partial\phi}-\lambda c\frac{\partial f_2}{\partial\phi}\right\}-\varepsilon^2|\nabla\phi|\kappa,$$

$$\frac{\partial c}{\partial t}=D\nabla^2 c+\frac{1}{2bk_c}\frac{\partial\phi}{\partial t}\left(1+\frac{D\nabla^2\phi-\partial\phi/\partial t}{k|\nabla\phi|}\right).$$

where:

$f_1(\phi)=-\frac{\phi^2}{2}+\frac{\phi^4}{4}$
$f_2(\phi)=\phi-\frac{\phi^3}{3}$
λ: coupling parameter
K: reaction rate
K_c: stoichiometric reaction rate, k_c = O(1)
b = C_s/rho

The formulation for reaction-rate, K, will be linked to whether the growth is kinetic limited or transport limited.

In general, whereas the aggregation results in fractal-looking structures, the surface growth tends to smooth the structure toward spherical-looking structures. The competition between these two mechanisms drives the ultimate morphology of the cluster. Notably, in the context of an integrated simulation framework, the "deposited phase," Φ, is effectively the same as the aggregated phase tracked in the DMC framework.

This integrated DMC/PFM framework is envisioned to be used to parametrically determine the evolution of cluster morphology as a function of local conditions (provided by the MD and LES frameworks). For example, Figure 11 shows the evolution of the fractal dimension and degree of surface anisotropy as a function of the background precursor concentration (i.e., equivalence ratio). The fractal dimension, D_f, is defined through the following:

$$n_p=\left(\frac{r_g}{r_p}\right)^{D_f};mr_g^2=\sum_{n_p}m_{p,i}r_i^2$$

where n_p is the number of primary particles in the cluster, and r_g and r_i correspond to the radius of gyration for the cluster and the radii of individual primary particles, respectively. The degree of anisotropy, A_{ij}, is defined through:

$$A_{ij}=\frac{R_i^2}{R_j^2},\ R_i>R_j..$$

where R_i is the principal radius of gyration (eigenvalue of MOI tensor). Figure 11 shows that as the equivalence ratio increases, the cluster tends to become more spherical, as indicated by increasing D_f and decreasing A_{ij}, in agreement with literature observations (Kireeva et al., 2009; Slowik et al., 2007), as shown in Figure 11.

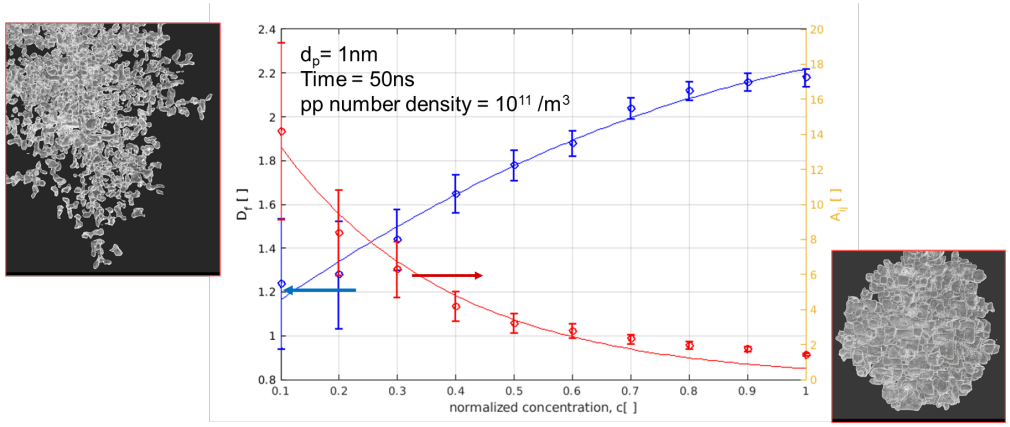

Figure 11. Variations in fractal dimension, D_f, and degree of anisotropy, A_{ij}, with background precursor concentration.

In another example, the evolution of the cluster morphology as function of primary particles number density is shown in Figure 12.

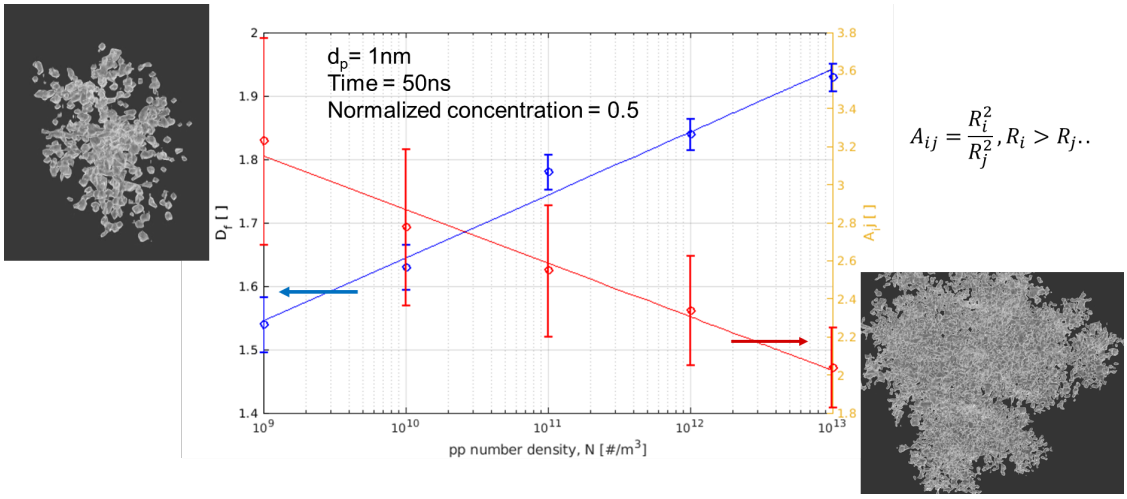

Figure 12. Variation of fractal dimension, D_f and degree of anisotropy, A_{ij} with number density of primary particles.

Although the cluster generally tends to be more symmetric and less fractal with increasing the primary particle number density, the variation tends to occur in a narrower range than the effect of precursor concentration.

Another important consideration is the role of short-range forces on the dynamics of aggregation. In classical DMC (Balthasar & Franklach, 2005; Mitchell & Franklach, 1998) the roles of short-term forces on the collision dynamics are often neglected. The collision probability is likely to be overestimated when those forces are repulsive and underestimated when the forces become attractive. Therefore, a simple force analysis is incorporated into the DMC framework to account for the short-range forces on particle trajectory and ultimately their aggregation behavior. In this approach, the Langevin motion equation is revised as follows:

$$\frac{dm\mathbf{u}}{dt} = -m\beta\mathbf{u} + \mathbf{f};\ \langle \mathbf{f^2} \rangle = 2\beta k_B T$$

The total stochastic force can now be decomposed into all relevant forces, pre-collision:

$$\mathbf{f} = \mathbf{f_{stoch}} + \mathbf{f_{VDW}} + \mathbf{f_e};\ \boldsymbol{S < S_{crit}}$$

The Van der Walls force, f_{VDW}, is estimated through simple Hamaker approximation:

$$\mathbf{f_{VDW}} = \frac{\mathrm{A_H} d_p}{2S^2}\hat{\mathbf{S}}$$

where d_p is the size of the particle, S is the distance between the particle and the aggregate, and A_H is the Hamaker constant (here, the value of A_H is 2.5 eV, corresponding to graphene–graphene interaction). The electrostatic force is approximated through the following:

$$\mathbf{f_e} = -\frac{1}{4\pi\epsilon}\frac{q_p q_c}{S^2}\hat{\mathbf{S}}$$

where q_c and q_p correspond to the charge density on the cluster and the primary particles, respectively. The approximation to this charge distribution is perhaps the weakest link in this approach and is expected to be more rigorous in the future. The charge distribution is approximated through empirical calculation of a correlation between the soot particles and measured charge density on the particles.

Inclusion of short-term forces substantially slows the progression from fractal to spherical morphology. For example, increasing precursor concentration tends to increase the fractal dimension but at a significantly slower rate than in the scenario in which those forces are neglected (Figure 13; triangles correspond to a dataset with short-term forces accounted for).

Blended Reaction

As noted previously, the reaction term in the PFM depends on whether the growth is kinetic-limited or transport-limited. In the former, the reaction rate is simply proportional to the size of the cluster:

$$r(t^n) = r(t^{n-1}) + \mathrm{k}\Delta t$$

Here, k is the reaction constant in units of m/s. In contrast, in a transport-limited regime, the growth also depends on background thermodynamic conditions (e.g., P and T). For the model to automatically transition from kinetic-limited to transport-limited growth, the phase-field formulation is recast with the coupling parameter, λ, now a function of cluster diameter, with the limit of the diameter approaching infinity. In the opposite limit, the reaction is assumed to reduce to a kinetic-limited regime:

$$\frac{dr}{dt} = K; r \to 0,\quad \frac{\tau\partial\Phi}{\partial t} = \epsilon^2\nabla^2\Phi - \frac{\partial f_1}{\partial\Phi} - \lambda(d)c\frac{\partial f_2}{\partial\Phi} - c^2|\nabla\Phi|k; r \to \infty$$

A matched asymptotic approach would lead to the following expression for $\lambda(d)$:

$$\lambda = \frac{d^3 c_\infty P}{K_B T\left(1 + \frac{dK}{D}\right)^{1+\frac{n}{2}}}$$

where P and T are background pressure and temperature, and c_∞ is the background concentration. This equation effectively determines the extent of coupling between the concertation field and the deposition field, which in turn determines the growth rate of the cluster. For example, at a temperature of 2000 K, the coupling parameter is plotted against the cluster diameter (normalized by mean-free-path length, l_{mft}, at the corresponding temperature and pressure) for different reaction constants in Figure 15.

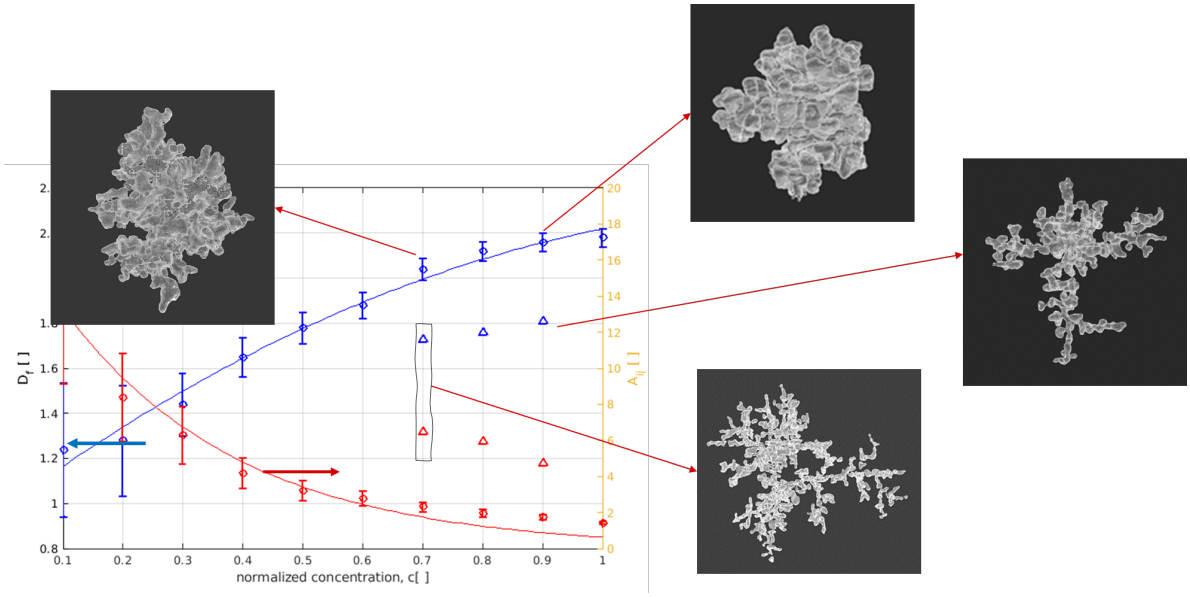

Figure 13. Variations in fractal dimension, D_f, and degree of anisotropy, A_{ij}, with background precursor concentration when short-range forces in the collision process are accounted for (triangles) vs. ignored (circles).

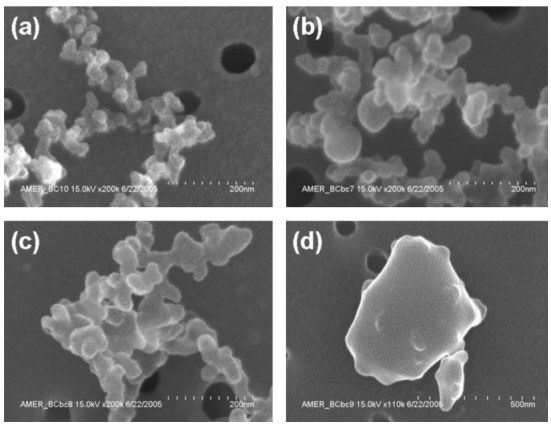

Figure 14. Scanning electron microscope (SEM) images of soot at four different equivalence ratios: ϕ = 2.3 (a), ϕ = 2.8 (b), ϕ = 3.5 (c), and ϕ = 5.0 (d).

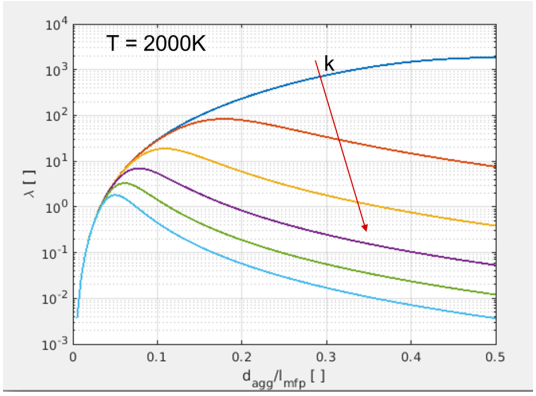

Figure 15. Variations in the coupling parameter in the PFM formulation as a function of aggregate size.

At small reaction constants, the growth consistently approaches that of transport-limited growth (strong coupling), whereas with sufficiently large reaction constants, the maximum coupling occurs at some small diameters, and the growth begins to recede back to that in the kinetic-limited regime.

Interestingly, particle growth is affected by shifting reaction regimes. Figure 16 shows the variations in particle morphology with time for non-dimensional reaction constant K_r (= K/K_c) = 0.01 as well as the ultimate fractal characteristics. The results indicate that the particles become consistently more spherical over time as the particle size (diameter) grows. However, at a larger reaction constant of K_r = 0.05 (Figure 17), a different trend is observed, and the fractal dimension peaks at $d_{agg} \approx 3$ nm and then starts to precipitously drop, thus indicating the dominance of kinetic-limited growth. Although this scenario might very well be only hypothetical, illustrating the evolution of the particle morphology under these regimes is nonetheless interesting.

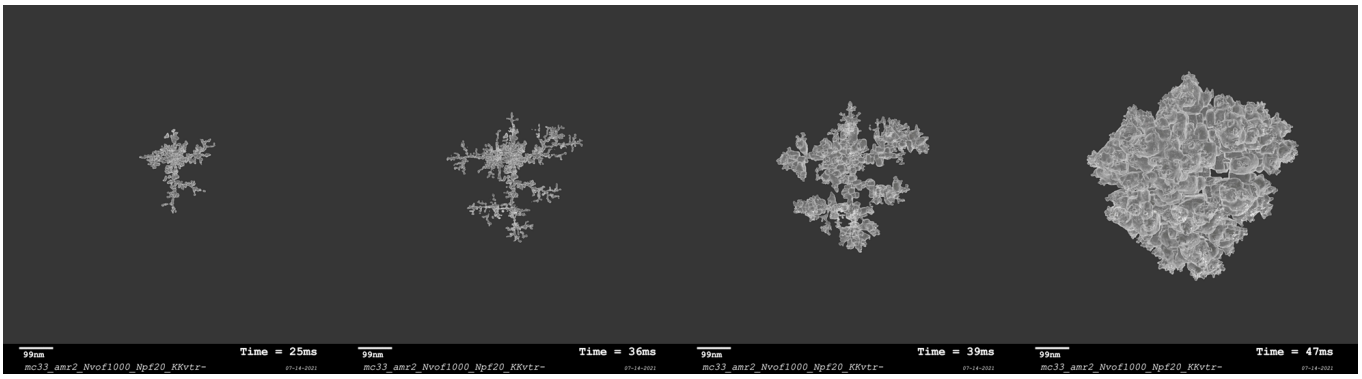

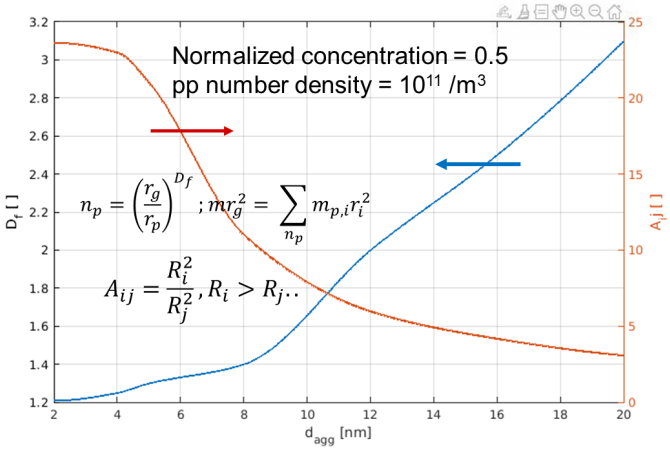

Figure 16. Snapshot of particle morphology at subsequent stages of growth (top), and variations in particle morphology with size (or time), with blended growth formulation with $K_r = 0.01$ (bottom).

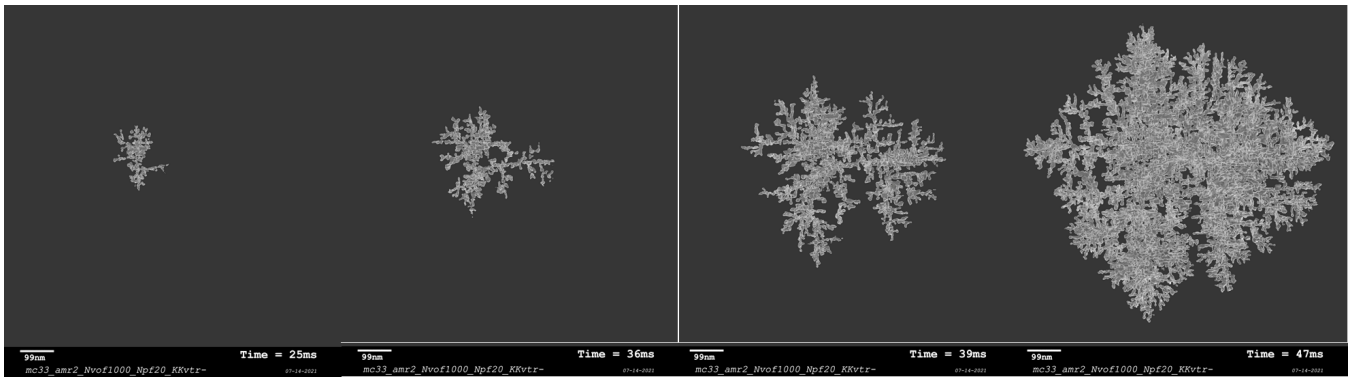

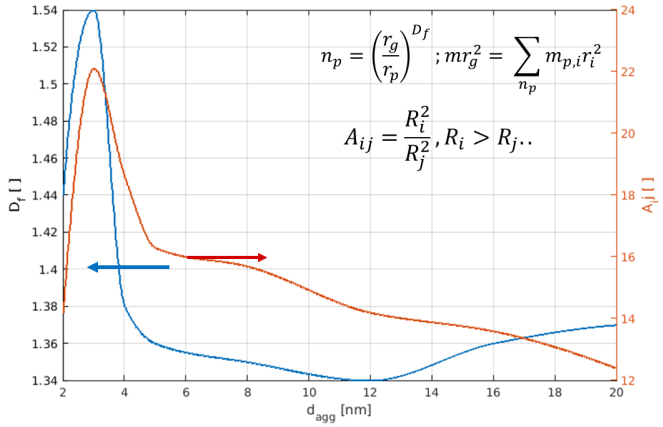

Figure 17. Snapshot of particle morphology at subsequent stages of growth (top), and variations in particle morphology with size (or time) with blended growth formulation with $K_r = 0.03$ (bottom).

Next Steps

- Completion of cluster–cluster agglomeration
- Computational acceleration for cluster–cluster agglomeration
- Coupling strategy for inception/post-inception model (MD)
- Coupling strategy for LES and definition of parametric space

Task 4 - Large Eddy Simulations

Georgia Institute of Technology

Objective

The objective of this task is to develop a physics-informed LES framework to model soot formation in turbulent reacting configurations of canonical and combustors of practical relevance. The current report discusses the LES-MOMIC and LEMLES-MOMIC frameworks to address large-scale simulations of soot modeling in turbulent reacting flows. The subsequent steps also included a collaboration with the kinetics group to include the effects of various mechanisms within the LES framework to address the sensitivity of soot precursor formation to chemistry effects. In future other team members will also be involved.

Research Approach

LES studies of turbulent sooting problems are very difficult because of the multiscale nature of soot inception, coagulation, and surface growth that must be modeled in a highly turbulent and reactive environment, typically in a complex combustor configuration. Most prior studies have focused on global models that approximate the small-scale physics. As such, many

available models account for the underlying physics. In contrast, simulations require some approximations, because the computational resources will never meet the simulation requirements. In the current effort, we balance contributing to the prediction of soot formation physics in a realistic gas turbine combustor with the need to obtain high-fidelity, reliable predictions by using advanced models. To achieve this goal, we leverage our past LES capability and upgrade the models by using the results from MD and MC studies. Soot evolution is tracked with MOMIC, wherein the first six moments of the particle size distribution function (PSDF) are used.

The full set of compressible reacting multispecies Navier–Stokes equations cannot be solved directly, because a direct numerical simulation is not feasible for practical applications. For LES, the large-scale flow features are resolved, and subgrid modeling is used for the smaller scales.

The LES governing equations can be written as follows:

$$\frac{\partial \bar{\rho}}{\partial t} + \frac{\partial}{\partial x_i}(\bar{\rho}\,\widetilde{u_\iota}) = 0$$

$$\frac{\partial}{\partial t}(\bar{\rho}\,\widetilde{u_\iota}) + \frac{\partial}{\partial x_j}\left(\bar{\rho}\,\widetilde{u_\iota}\,\widetilde{u_j} + \bar{P}\,\delta_{ij} - \overline{\tau_{\iota J}} + \tau_{ij}^{sgs}\right) = 0$$

$$\frac{\partial}{\partial t}\left(\bar{\rho}\,\tilde{E}\right) + \frac{\partial}{\partial x_j}\left[\left(\bar{\rho}\,\tilde{E} + \bar{P}\right)\widetilde{u_\iota} + \overline{q_\iota} - \widetilde{u_J}\,\overline{\tau_{\iota J}} + H_i^{sgs} + \sigma_i^{sgs}\right] = 0$$

$$\frac{\partial}{\partial t}\left(\bar{\rho}\,\widetilde{Y_k}\right) + \frac{\partial}{\partial x_j}\left[\bar{\rho}\,\widetilde{Y_k}\,\widetilde{u_j} - \bar{\rho}\,\overline{D_k}\,\frac{\partial \widetilde{Y_k}}{\partial x_j} + \Phi_{j,k}^{sgs} + \Theta_{jk}^{sgs}\right] = \bar{\rho}\,\widetilde{\dot{w}_k}$$

$$\frac{\partial}{\partial t}\left(\bar{\rho}\,\widetilde{Y_{soot}}\right) + \frac{\partial}{\partial x_j}\left[\bar{\rho}\,\tilde{Y}_{soot}\,\widetilde{u_j} - \bar{\rho}\,\bar{D}_{soot}\,\frac{\partial \tilde{Y}_{soot}}{\partial x_j} + \widetilde{V_T}_{soot}\,\tilde{Y}_{soot} + \Phi_{j,k,soot}^{sgs} + \Theta_{jk,soot}^{sgs}\right] = \bar{\rho}\,\widetilde{\dot{w}}_{soot}$$

$$\frac{\partial}{\partial t}\left(\bar{\rho}\,\widetilde{M_k}\right) + \frac{\partial}{\partial x_j}\left[\bar{\rho}\,\widetilde{M_k}\,\widetilde{u_j} - \bar{\rho}\,\bar{D}_{soot}\,\frac{\partial \widetilde{M_k}}{\partial x_j} + \widetilde{V_T}\,\widetilde{M_k} + \Psi_{j,k}^{sgs} + \Omega_{j,k}^{sgs}\right] = \bar{\rho}\,\widetilde{\dot{M}_k}$$

Here, $\widetilde{u_\iota}$ is the *i*-th filtered velocity, $\bar{\rho}$ is the filtered density, and $\bar{P}$ is the filtered pressure, which is computed from the filtered equation of state. $\tilde{T}$ is the filtered temperature, $\tilde{E}$ is the filtered energy, and $\widetilde{Y_k}$ and $\widetilde{Y}_{soot}$ represent the filtered *k*-th gas-phase species and soot mass fraction, respectively, and $\widetilde{M_k}$ represents the *k*-th moments of the PSDF. The details regarding the computations of all these quantities have been described elsewhere (El-Asrag & Menon, 2009) and hence are not discussed herein in specific detail. The filtered heat flux $\bar{q}$ can be supplied to an optically thin radiation model to include effects of radiation. The terms $\tau_{ij}^{sgs}, H_i^{sgs}, \sigma_i^{sgs}, \Phi_{j,k}^{sgs}, \Theta_{j,k}^{sgs}, \Psi_{j,k}^{sgs}$, and $\Omega_{j,k}^{sgs}$ contain the effects of the subgrid scale on the filtered quantities. Modeling of these terms remains challenging; in addition, the closed system of equations must be solved together in three-dimensional space with temporal accuracy.

In this work, an eddy viscosity type subgrid model with constant coefficients is used to obtain the closure of subgrid momentum stresses and subgrid enthalpy flux. In the linear eddy mixing (LEM) formulation, the gas-phase species conservation equations are not spatially filtered as in other LES equations. Instead, the exact unfiltered equations are solved by using a two-scale, two-step Eulerian–Lagrangian approach. First, within each LES cell, the one-dimensional LEM model is used to solve for the scalar fields (species mass fraction, soot mass fraction, LEM temperature, and soot integer moments) along a notional line oriented along the maximum scalar gradient. Second, the subgrid scale fields are convected across the LES cell faces by using a Lagrangian transport approach through the splicing algorithm, which reproduces the effect of large-scale advection of the scalars by the flow field. The resulting scalar fields are then filtered in each LES cell to recover LES-resolved species mass fractions to be used in LES-resolved energy and state equations. More details regarding the original LEMLES formulation and its extension to account for soot dynamics through the MOMIC approach have been described elsewhere and are briefly described herein.

The one-dimensional LEM-MOMIC takes the following form:

$$\rho \frac{\partial Y_k}{\partial t} = F_k + \frac{\partial}{\partial s}\left(\rho D_k \frac{\partial Y_k}{\partial s}\right) + \dot{w}_k$$

$$\rho \frac{\partial Y_{soot}}{\partial t} = F_{soot} + \frac{\partial}{\partial s}\left(\rho D_{soot} \frac{\partial Y_{soot}}{\partial s} - V_{T,soot}\, Y_{soot}\right) + \dot{\omega}_{soot}$$

$$\frac{\partial T}{\partial t} = F_T - \frac{1}{\overline{C_p}} \Sigma_{k=1,N_s}\left(C_{p,k} Y_k V_k \frac{\partial T}{\partial s}\right) + \frac{1}{\rho\, \overline{C_p}}\left(\frac{\partial}{\partial s}\left(\bar{k}\frac{\partial T}{\partial s}\right)\right) - \frac{1}{\rho\, \overline{C_p}} \Sigma h_k\, \dot{\omega}_k W_k + a_{over}\sigma(T^4 - T_o^4)$$

$$\frac{\partial M_r}{\partial t} = R_r + C_r + S_r + F_{M_r}$$

In the above equations, Y_k and Y_{soot} are the *k*-th gas-phase species and soot mass fractions, respectively, which are subjected to the mass conservation condition $\Sigma Y_k + Y_{soot} = 1.0$. The soot molecular diffusivity and thermophoretic velocity are denoted by D_{soot} and $V_{T,soot}$ respectively. The temperature equation is supplied with an optically thin radiation model. Here, $F_k, F_{soot}, F_T,$ and F_{M_r} all denote the effects of subgrid turbulence in the gas-phase species, soot mass fraction, temperature, and moments, respectively. In the current formulation, F_{M_r} is neglected, to account for the effect of turbulence on soot. The F_{soot} term is modeled through turbulent stirring operations in the same manner as for other species.

The remaining terms, $R_r, C_r,$ and S_r, represent the soot moment source terms from the nucleation, coagulation, and surface growth, respectively. These terms are modeled with a MOMIC approach. In method of moments, the Smoluchowski equations describing the population dynamics of a system of particles are rewritten in terms of the moments of the PSDF. The PSDF can also be described by its moments, and most practical application properties can be easily estimated from its first few moments. The moments are defined as $M_r = \Sigma m_i^r N_i$, where M_r is the *r*-th moment, and m_i and N_i are the masses and number density of particles with size *i*. Therefore, method of moments is useful because it replaces an infinite sequence of equations with a set of a few equations to estimate properties of practical interest. The zeroth moment, M_0, represents the soot number density, N_S, defined by the number of soot particles per unit volume of the mixture. The first moment, M_1, represents the average total mass of soot particles, m_S, per unit volume. Thus, the soot mass fraction is $Y_S = M_1/\rho$, where ρ is the mixture density. The average particle diameter $d_p = (6.0M_2/\pi\rho_{soot}M_1)^{1/3}$ (El-Asrag & Menon, 2009; Srinivasan & Menon, 2015).

The following key inputs have been identified for improvements in the existing MOMIC model, in collaboration with other cost-share partners:

1) The current MOMIC model uses the Lindstedt four-step soot kinetic model to model the kinetic rates of soot nucleation, surface growth, and oxidation. This kinetic model uses the empirical constants highlighted in Figure 3. The inputs from the RTRC kinetic group regarding the empirical constants must be incorporated in the source terms of nucleation and surface growth terms.
2) The current LES-MOMIC and LEMLES-MOMIC approaches use reduced chemical kinetics (19-species, 15-step ethylene–air kinetics developed by Lu and coworkers). However, the kinetics lacks information on the aromatic species and is not designed to work under the high-pressure conditions in practical gas turbine combustors.
3) The nucleation in the current code is based on the assumption that acetylene is a gas-phase soot precursor, which is reasonable for ethylene flames. However, for aviation fuels, it has been found that aromatic species are key in the formation of early soot incipient nuclei. The MD studies performed at UM in close association with the RTRC kinetic group provide information on the kinetic rates of formation of these aromatic dimers. This effect needs to be included in the current MOMIC approach.
4) In the non-coalescent regime, the MOMIC source terms for aggregate formation require information on the fractal dimension of these aggregates as a function of background gas-phase conditions. The MC studies of the RTRC surface growth modeling team provide information on fractal dimensions as a parametric function of sensitive background conditions and can be fed into the MOMIC code in LES framework.

In the last annual effort, assessment of the existing MOMIC approach to account for first six moments of the soot particle size distribution function were performed. Various one-dimensional tests were performed to verify the implementation of

MOMIC. Further, soot formation in a laminar flame by using reduced ethylene 19-species, 15-step kinetics coupled with a four-step Lindstedt soot kinetic model was compared with the experimental results from Xu and Faeth (2001). In the current effort, the primary task was to establish methodology for soot evolution in turbulent flames, accounting for the effects of turbulence on soot formation processes. In a demonstration, a three-dimensional premixed rich C_2H_4/air flame interacting with background turbulence is used. The proposed test intends to use the LEMLES-MOMIC model with finite rate chemistry for the premixed flame turbulence interaction problem (El-Asrag et. al., 2007) under the conditions in Table 1.

Table 1. Turbulence and flame parameters.

u'	l_{11}	Re_λ	s_l
1.67 m/s	1.475 mm	156	0.167 m/s

The schematic of the configuration is shown in Figure 18. The premixed C_2H_4/air mixture enters the inlet at $\varphi = 2.33$, at P_{ref} = 1 atm and T_{ref} = 300 K. According to the inflow conditions, the laminar flame speed (S_l) is 0.167 m/s. Turbulence parameters (u', l_{11}) are chosen such that the flame is in the thin reaction zone (TRZ) regime. The initial flame front is obtained from the laminar premixed flame solution and is specified at the center of the domain, with the left side denoting the reactants and the right side denoting the products. The extent of the computational domain is 15 mm × 15 mm × 15 mm in the streamwise *x*, transverse *y*, and spanwise *z* directions. The flow field is initialized by using the von Karman–Pao energy spectrum. Characteristic inflow–outflow conditions are specified in the streamwise direction, whereas periodic conditions are specified in the other two directions. The LES grid resolution chosen for the simulations is 64 × 64 × 64 LES cells. LEM is used to account for subgrid turbulence–chemistry closure. A total of 12 LEM cells are chosen in each LES, so that subgrid effects until Kolmogorov's length scale can be resolved.

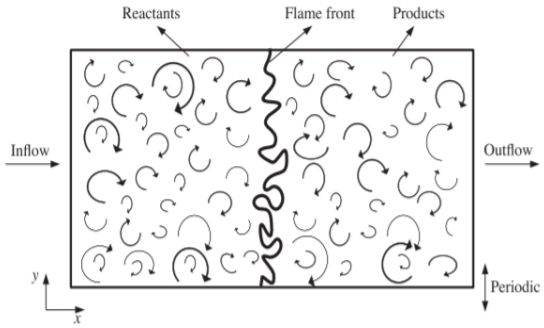

Figure 18. Schematic of premixed flame–turbulence interaction.

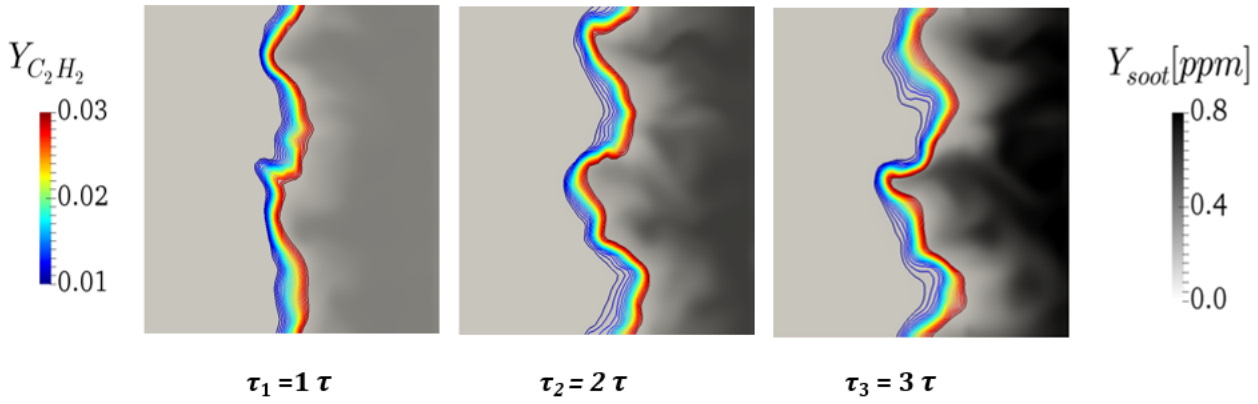

Figure 19. Soot mass fractions overlapped with C_2H_2 contours.

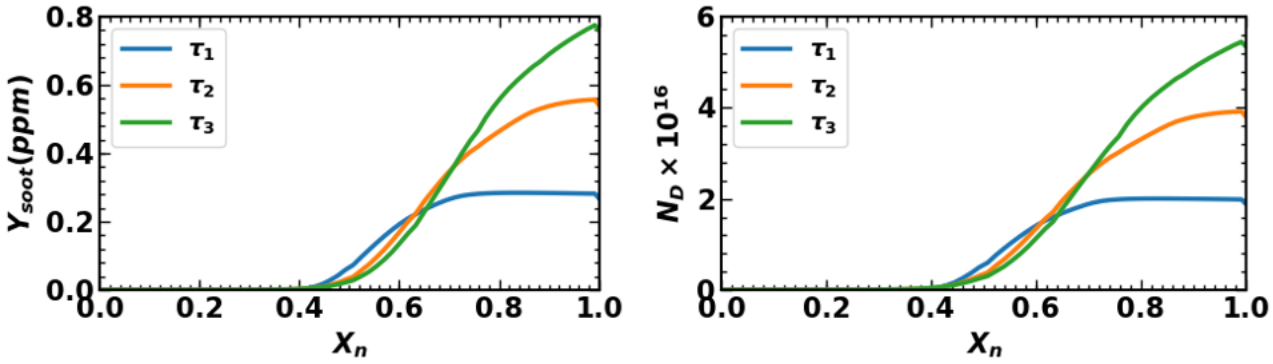

Figure 20. Planar average of Y_{soot} and number density profile along the flame normal directions ($\tau_1 = \tau_{eddy}$, $\tau_2 = 2\tau_{eddy}, \tau_3 = 3\tau_{eddy}$).

The time evolution contours of the soot mass fraction are shown in Figure 19. As can be seen, the presence of background turbulence severely deforms the initially laminar planar flame front. The rich premixed ethylene mixture decomposes, forming acetylene, which acts as a soot precursor. The acetylene molecules break down further and form soot nuclei. The increasing soot mass fraction and number density with eddy turnover time ($\tau_{eddy} = \frac{u'}{s_l}$) are evident in Figure 20. The LEMLES-MOMIC approach is demonstrated only with nucleation. The effects of radiation and agglomeration are also neglected at this stage (but will be reconsidered later).

The initial study included a collaboration with the kinetics group at RTRC to incorporate the skeletal chemistry in the LES framework and assess the effects of chemistry in predicting key gas-phase precursor species (C_2H_2). To do so, the premixed flame turbulence interaction problem described above is revisited but without the inclusion of soot species, i.e., only gas-phase species are simulated by using two different mechanisms:

Mechanism A (reduced chemistry): 19-species, 15-step reduced mechanism developed by Lu and coworkers
Mechanism B (skeletal chemistry): 33-species, 206-step skeletal mechanism developed by Lu and coworkers, assessed by the RTRC kinetic group.

Initially, the timescales of production of each species are estimated for both chemistries and are plotted in a bar chart in Figure 21. As shown, the skeletal chemistry is stiffer than the reduced chemistry (timescales of some species are on the order of 1×10^{-7}); however, the species are still well resolved with the current LES timescale. The spanwise averages of the fuel decomposition rate (C_2H_4) as well as precursor (C_2H_2) production rates with respect to the filtered progress variables obtained with both mechanisms are plotted in Figure 22. The reduced mechanism, compared with the skeletal mechanism, predicts mass fractions that are approximately two times greater possibly due to the inclusion of aromatic pathways in the pyrolysis of fuel. These inputs are conveyed to the kinetics group, which will conduct further assessment of the kinetics with different detailed mechanisms to establish a confidence interval for prediction of the soot precursor species under different operating conditions.

Next Steps

- Inclusion of nucleation from UM into the LES approach
- Extension of LES models to include radiation and agglomeration models from RTRC
- Validation of LES to canonical sooting flames
- Evaluation of model for PAH pathways for soot formation
- Evaluation of aggregation models using LES data

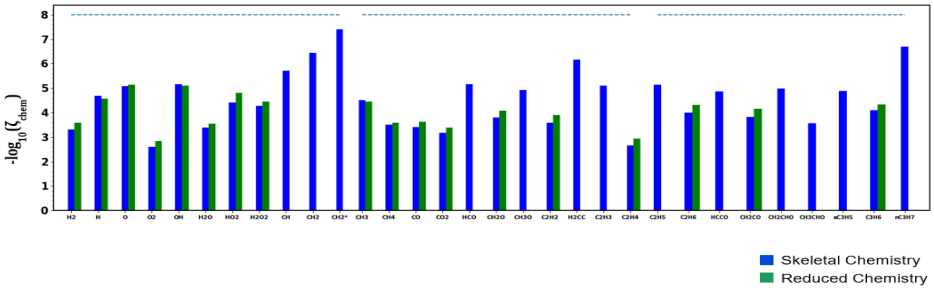

Figure 21. Comparison of chemical timescales for species involved in reduced and skeletal chemistries.

The *y* axis is the negative of the species production timescale. The dotted blue horizontal line is the typical LES timescale. Almost all species present in skeletal and reduced chemistry lie below the blue dotted line, thus suggesting that the LES timescale is less than all the chemical timescales.

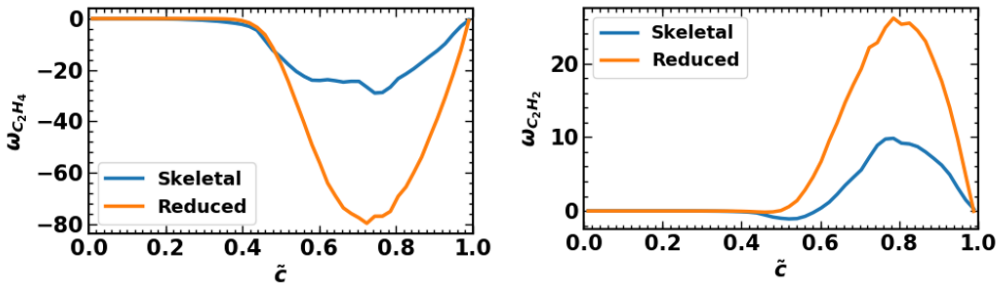

Figure 22. Comparison of consumption rates for reactants and production rates for soot precursors, with reduced and skeletal chemistry.

Milestone(s)

Milestone	Planned Due Date
Improvements in the Lindstedt soot kinetic model	12/31/2021
Development of reduced kinetics for PAH chemistry	3/31/2022
MD simulation framework for dimer stability	3/31/2022
MC simulation for surface growth and cluster–cluster aggregation	3/31/2022
LES-MOMIC and LEMLES-MOMIC frameworks for soot–turbulence–chemistry assessment	3/31/2022

Major Accomplishments

- Improvements in the four-step Lindstedt soot kinetic model to predict reduced rates at higher temperatures
- Development of reduced kinetics including PAH pathways
- MD simulations for pools of PAH rings at a range of flame temperatures
- Framework for reaction- and transport-limited growth of soot particles, as well as models for cluster–cluster aggregation
- LEMLES-MOMIC numerical framework for soot–turbulence–chemistry interactions

Publications

Saldinger, J. C., Elvati, P., & Violi, A. (2021). Stochastic and network analysis of polycyclic aromatic growth in a coflow diffusion flame. Physical Chemistry Chemical Physics, *23*(7), 4326-4333.

Outreach Efforts

None

Awards

None

Student Involvement

Shubham Karpe, PhD student, has been assisting with the development of the MOMIC framework within the LES code at Georgia Tech. Another student is working on the UM team.

Plans for Next Period

Kinetics activities at RTRC

The next quarterly efforts will focus on refining the reduced chemistry developed with PAH species, with particular attention paid to extending the predictions and validation over a wide range of conditions. The reduced kinetics will be provided to Georgia Tech, and the information on the gas phase will be provided to UM for nucleation studies.

MD Simulations at UM

Future activities in this work will focus on expanding the pool of PAHs to consider the effects of heavier monomers, impact of aliphatic chains, and oxygen radicals on the stability of dimer formations. The inputs regarding the global nucleation rates from these studies will be provided to GT to improve source terms in the 6-MOMIC approach.

Surface Growth Modeling at RTRC

Studies are underway to consider models for full cluster–cluster aggregation. The information regarding the primary soot nuclei (size and distributions) from MD simulations at UM, and regarding local conditions from LES studies at Georgia Tech, will be included in current growth models at RTRC. The outputs regarding the fractal dimensions and anisotropy of aggregates will be provided to Georgia Tech for their MOMIC model.

LES Studies at Georgia Tech

The next set of activities at Georgia Tech will involve incorporating the reduced ethene kinetics with PAH species and the soot kinetic model at RTRC to improve the existing soot model. The extinction–reignition setup based on DNS studies (Lignell et. al., 2008) will be explored to study soot formation and transport in non-premixed jet flames by using LES-MOMIC and later LEMLES-MOMIC. The inputs from fundamental studies at RTRC and UM will be included to improve the architecture of the existing MOMIC model, which will be further compared in premixed and non-premixed canonical ethylene–air flames.

References

Balthasar, M., & Frenklach, M. (2005). Monte-Carlo simulation of soot particle coagulation and aggregation: the effect of a realistic size distribution. Proceedings of the Combustion Institute, *30*(1), 1467–1475. https://doi.org/10.1016/j.proci.2004.07.035

Chen, J.-Y. (1988). A general procedure for constructing reduced reaction mechanisms with given independent relations. Combustion Science and Technology, *57*(1-3), 89–94. https://doi.org/10.1080/00102208808923945

Colket, M. B., Hall, R. J., & Stouffer, S. D. (2004, June 14-17). Modeling soot formation in a stirred reactor [Presentation]. Proceedings of the ASME Turbo Expo 2004: Power for Land, Sea, and Air, Vienna, Austria. https://doi.org/10.1115/GT2004-54001

Glarborg, P., Kee, R. J., Grcar, J. F., & Miller, J. A. (1986). PSE: a Fortran program for modeling well-stirred reactors (Report No. SAND86-8209). Sandia National Laboratories, Livermore, CA.

El-Asrag, H., & Menon, S. (2009). Large eddy simulation of soot formation in a turbulent non-premixed jet flame. Combustion and Flame, *156*(2), 385–395. https://doi.org/10.1016/j.combustflame.2008.09.003

El-Asrag, H., Lu, T., Law, C. K., & Menon, S. (2007). Simulation of soot formation in turbulent premixed flames. Combustion and Flame, *150*(1-2), 108–126. https://doi.org/10.1016/j.combustflame.2007.01.005

Frenklach, M. (2002). Method of moments with interpolative closure. Chemical Engineering Science, *57*(12), 2229–2239. https://doi.org/10.1016/s0009-2509(02)00113-6.

Kireeva, E. D., Popovicheva, O. B., Persiantseva, N. M., Timofeyev, M. A., & Shonija, N. K. (2009). Fractionation analysis of transport engine-generated soot particles with respect to hygroscopicity. Journal of Atmospheric Chemistry, *64*(2-3), 129–147. https://doi.org/10.1007/s10874-010-9173-y

Leung, K. M., Lindstedt, R. P., & Jones, W. P. (1991). A simplified reaction mechanism for soot formation in nonpremixed flames. Combustion and Flame, *87*(3-4), 289–305. https://doi.org/10.1016/0010-2180(91)90114-q

Lignell, D. O., Chen, J. H., & Smith, P. J. (2008). Three-dimensional direct numerical simulation of soot formation and transport in a temporally evolving nonpremixed ethylene jet flame. Combustion and Flame, *155*(1-2), 316–333. https://doi.org/10.1016/j.combustflame.2008.05.020

Lu, T., & Law, C. K. (2005). A directed relation graph method for mechanism reduction. Proceedings of the Combustion Institute, *30*(1), 1333–1341. https://doi.org/10.1016/j.proci.2004.08.145

Mitchell, P., & Frenklach, M. (1998). Monte Carlo simulation of soot aggregation with simultaneous surface growth-why primary particles appear spherical. Symposium (International) on Combustion, *27*(1), 1507–1514. https://doi.org/10.1016/s0082-0784(98)80558-4

Saldinger, J. C., Elvati, P., & Violi, A. (2021). Stochastic and network analysis of polycyclic aromatic growth in a coflow diffusion flame. Physical Chemistry Chemical Physics, *23*(7), 4326–4333. https://doi.org/10.1039/d0cp03529g

Slowik, J. G., Cross, E. S., Han, J.-H., Davidovits, P., Onasch, T. B., Jayne, J. T., Williams, L. R., Canagaratna, M. R., Worsnop, D. R., Chakrabarty, R. K., Moosmüller, H., Arnott, W. P., Schwarz, J. P., Gao, R.-S., Fahey, D. W., Kok, G. L., & Petzold, A. (2007). An inter-comparison of instruments measuring black carbon content of soot particles. Aerosol Science and Technology, *41*(3), 295–314. https://doi.org/10.1080/02786820701197078

Srinivasan, S., & Menon, S. (2015). Soot modeling using the linear eddy model (Report No. CCL-TR-2015-03-10)., Environmental Protection Agency.

Stouffer, S., Striebich, R. C., Frayne, C. W., & Zelina, J. (2002, July 12-17). Combustion Particulates Mitigation Investigation Using a Well-Stirred Reactor [Presentation]. 38th AIAA/ASME/SAE/ASEE Joint Propulsion Conference & Exhibit, Indianapolis, IN.

Sun, Y., & Beckermann, C. (2007). Sharp interface tracking using the phase-field equation. Journal of Computational Physics, *220*(2), 626–653. https://doi.org/10.1016/j.jcp.2006.05.025

Xu, F., & Faeth, G. M. (2001). Soot formation in laminar acetylene/air diffusion flames at atmospheric pressure. Combustion and Flame, 125(1-2), 804–819. https://doi.org/10.1016/s0010-2180(01)00221-8

Xu, Z., & Meakin, P. (2008). Phase-field modeling of solute precipitation and dissolution. The Journal of Chemical Physics, *129*(1), 014705. https://doi.org/10.1063/1.2948949